

Finite temperature expansion dynamics of Bose-Einstein condensates

Arko Roy and D. Angom

Physical Research Laboratory, Ahmedabad - 380009, Gujarat, India

(Dated: November 15, 2018)

We explore the effects of finite temperature on the dynamics of Bose-Einstein condensates (BECs) after it is released from the confining potential. In addition, we examine the variation in the expansion dynamics of the BECs as the confining potential is transformed from a multiply to a simply connected geometry. To include the effects of finite temperatures we use the frozen thermal cloud approximation, and observe unique features of the condensate density distribution when released from the confining potential. We find that at $T \neq 0$, during the initial stages of expansion, the multiply connected condensate has more pronounced interference rings compared to the case of zero temperature. Such difference in the dynamical evolution is also evident for simply connected condensates.

PACS numbers: 03.75.Kk, 67.85.De, 03.75.Hh

I. INTRODUCTION

The time-of-flight measurement is an important experimental technique to detect Bose-Einstein condensation in dilute atomic gases, and probe their other properties as well. In this technique the atoms are left to expand by switching off the external confining potential, and the atoms are then imaged with optical methods. The technique has been used to observe a plethora of diverse phenomena in the Bose-Einstein condensates (BECs) of dilute atomic gases. Few examples are the experimental observation of the non-equilibrium many-body phenomenon based on matter wave interference patterns [1], and the observation of thermally activated vortex pairs in a quasi-2D Bose gas leading to a crossover from a Berezinskii-Kosterlitz-Thouless phase to a vortex-free BEC [2]. In fermionic atomic species, the technique has been used to probe the superfluidity of strongly interacting Fermi mixtures [3] and, to measure the p -wave Feshbach resonances for fermionic atoms [4].

Toroidal condensates, which are multiply connected BECs, are near ideal systems to study phenomena related to persistent superflows. In these systems too, the time-of-flight measurements play an important role to detect and probe the phenomena of interest. In experiments, toroidal condensates have been obtained with the use of harmonic potential in combination with a Gaussian potential [5], Laguerre-Gaussian beams [6–9], combination of an RF-dressed magnetic trap with an optical potential [10, 11], magnetic ring traps [12–15], time-averaged ring potentials [16, 17], coincident red and blue detuned laser beams [18], and employing digital micromirror devices [19]. The toroidal or ring condensates also serve as model-systems in the field of atomtronics. These systems have been used to implement superconducting quantum interference devices (SQUIDs) [20, 21], and phase-slips in rf SQUID have been modelled by employing blue-detuned laser beam along the axis of toroidal condensates [22]. In both of these experiments, the phase-difference along the condensate has been measured from the free expansion dynamics. It is found that for toroidal BECs with finite circulation the images after expansion have a central hole whose area is proportional to the winding number. On the other hand, there is finite density at the center when there is no circulation [22, 23].

These are well understood and in good agreement with theoretical simulations using zero temperature time-dependent Gross-Pitaevskii (GP) equation [23].

For the present work, we consider a toroidal BEC obtained with a confining potential consisting of a harmonic and Gaussian potential [5]. This configuration offers the possibility to probe the effects associated with the transition from multiply to simply connected BEC due to relative shift in the component trapping potentials. In experiments, this is an important consideration since the trap centers, extremum of the harmonic and Gaussian trapping potentials, never coincide. This is due to gravitational sagging, and deviations of the optical elements and external fields from perfect alignment. In addition, it is worth mentioning that, in experiments, the drift due to thermal cycling alone transforms the multiply to simply connected BEC [5]. These experimental realities establish the need to theoretically probe the effects of geometry on the expansion dynamics of a quasi-2D BEC. To validate the experimental results, and considering the deviations from an ideal case, it is also pertinent to examine the role of thermal fluctuations on the expansion dynamics. So that, it is possible to distinguish and identify the effects of relative shift in the trapping potential, and those emerging from the thermal fluctuations.

To examine the thermal fluctuations in the toroidal BEC as a function of the separation between the trap centers we use the Hartree-Fock-Bogoliubov theory with Popov (HFB-Popov) approximation. The increase in the separation of the trap centers induces a topological transformation in the condensate density profiles. The condensate density profile is modified from toroidal or multiply connected to a bow-shaped or simply connected geometry, the profile of the quantum fluctuations also exhibit a similar transformation. The thermal fluctuations, in contrast, remain multiply connected [24]. These differences in the structure of the condensate and thermal density profiles affect the dynamics of the condensate cloud during expansion at finite temperature. We examine this in detail using frozen thermal cloud approximation. It is to be mentioned here that, previous works using the classical field approximation have shown that thermal fluctuations affect the radial and axial condensate widths during expansion [25, 26].

II. THEORETICAL METHODS

The grand-canonical Hamiltonian of an interacting quasi-2D BEC system is

$$\hat{H} = \iint dxdy \hat{\Psi}^\dagger(x, y, t) \left[-\frac{\hbar^2}{2m} \left(\frac{\partial^2}{\partial x^2} + \frac{\partial^2}{\partial y^2} \right) + V(x, y) - \mu + \frac{U}{2} \hat{\Psi}^\dagger(x, y, t) \hat{\Psi}(x, y, t) \right] \hat{\Psi}(x, y, t). \quad (1)$$

where $\hat{\Psi}$ and μ are the Bose field operator of a scalar BEC, and the chemical potential, respectively. We consider an external confining potential of the form $V(x, y) = (1/2)m\omega_x^2(x^2 + y^2 + \lambda^2 z^2) + U_0 e^{-[(x-\Delta_x)^2 + y^2]/2\sigma^2}$, which is a superposition of the harmonic oscillator and Gaussian potential with strength U_0 . This choice of the potential parameters implies that the aspect ratio in the transverse direction $\alpha = \omega_y/\omega_x = 1$. The case of $U_0 = 0, \Delta_x = 0$ then produces a symmetric 2D harmonic trap, whereas $U_0 \gg 0$ makes it a toroid. Let Δ_x represent the separation between the centers of the harmonic and Gaussian potentials, we can consider the separation as along the x -axis through an appropriate rotation of the coordinates. This separation accounts for the non-coincidence of the trapping potential centers. This deviation is natural, since in experiments trap centers never coincide because of gravitational sagging, and optical axes are not perfectly aligned. In a quasi-2D system, as $\omega_z \gg \omega_x$ the condensate is considered to be in the ground state along z , and the excitations along the transverse direction only contribute to the dynamics. The atoms of the bosonic species with mass m and scattering length a interact repulsively through the s -wave binary collisions with strength $U = 2a\sqrt{2\pi}\lambda$.

A. Gapless Hartree-Fock-Bogoliubov-Popov formalism

To compute the equilibrium density profiles of BEC at finite temperatures, we use the gapless HFB-Popov theory. In this theory the Bose field operator $\hat{\Psi}$ is decomposed into a condensate part represented by $\phi(x, y, t)$, and the fluctuation part denoted by $\tilde{\psi}(x, y, t)$. That is $\hat{\Psi} = \phi + \tilde{\psi}$, and the condensate part $\phi(x, y, t)$ solves the generalized GP equation

$$\hat{h}\phi + U[n_c + 2\tilde{n}]\phi = 0. \quad (2)$$

In the above equation the single-particle or the non-interacting part of the Hamiltonian is $\hat{h} = (-\hbar^2/2m)(\partial^2/\partial x^2 + \partial^2/\partial y^2) + V(x, y) - \mu$ with $n_c(x, y) \equiv |\phi(x, y)|^2$, $\tilde{n}(x, y) \equiv \langle \tilde{\psi}^\dagger(x, y, t) \tilde{\psi}(x, y, t) \rangle$, and $n(x, y) = n_c(x, y) + \tilde{n}(x, y)$ as the local condensate, non-condensate or thermal, and total density, respectively. To determine the non-condensate density, the fluctuation operator $\tilde{\psi}$ is represented through a superposition of Bogoliubov quasiparticle as

$$\tilde{\psi} = \sum_j \left[u_j(x, y) \hat{\alpha}_j(x, y) e^{-iE_j t/\hbar} - v_j^*(x, y) \hat{\alpha}_j^\dagger(x, y) e^{iE_j t/\hbar} \right],$$

with j denoting the energy eigenvalue index of a quasiparticle mode having energy E_j . The quasiparticle annihilation (creation) operators $\hat{\alpha}_j$ ($\hat{\alpha}_j^\dagger$) satisfy the usual Bose commutation relations. The functions u_j and v_j are the Bogoliubov quasiparticle amplitudes corresponding to the j th energy eigenstate, and solves the following pair of coupled Bogoliubov-de Gennes (BdG) equations

$$(\hat{h} + 2Un)u_j - U\phi^2 v_j = E_j u_j, \quad (4a)$$

$$-(\hat{h} + 2Un)v_j + U\phi^{*2} u_j = E_j v_j. \quad (4b)$$

Following these definitions, the thermal or the non-condensate density at temperature T is

$$\tilde{n} = \sum_j \{ [|u_j|^2 + |v_j|^2] N_0(E_j) + |v_j|^2 \}, \quad (5)$$

where $\langle \hat{\alpha}_j^\dagger \hat{\alpha}_j \rangle = (e^{\beta E_j} - 1)^{-1} \equiv N_0(E_j)$ with $\beta = 1/k_B T$, is the Bose factor of the j th quasiparticle state with energy E_j at temperature T . More details of the derivations, and numerical scheme to solve the generalized GP and coupled Bogoliubov-de Gennes (BdG) equations self-consistently are given in our previous works [24, 27–29].

B. Frozen thermal cloud approximation

To study the dynamics of BEC at finite temperatures, we solve the time dependent GP equation with frozen thermal cloud approximation. In this approximation the dynamics of the thermal cloud is ignored, and the condensate atoms move in the presence of a static cloud of non-condensate atoms which are in a state of thermal equilibrium with the initial state, and obeys Bose-Einstein distribution function. This, in the expansion dynamics of the condensate after the removal of the trapping potential, is equivalent to introducing a perturbation potential to the condensate atoms when $T > 0$. The total number of atoms during the evolution is conserved, in other words there is no transfer of atoms between the condensate and thermal clouds. Thus the dynamics of the order parameter ϕ of the BEC under frozen thermal cloud approximation follows the equation

$$i\hbar \frac{\partial \phi}{\partial t} = \left[-\frac{\hbar^2}{2m} \nabla_\perp^2 + 2U\tilde{n} + Un_c \right] \phi(x, y, t). \quad (6)$$

Here $\nabla_\perp^2 = \partial^2/\partial x^2 + \partial^2/\partial y^2$, and U is interaction strength as defined earlier. The time independent interaction with the thermal density \tilde{n} acts as an effective potential in which the condensate moves. To probe the region of validity of this approximation we compute the velocity of the thermal cloud through the computation of root mean square value of wave vector

$$k_{\text{th}}^{\text{rms}} = \left\{ \frac{\iint dk_x dk_y (k_x^2 + k_y^2) \tilde{n}(k_x, k_y)}{\iint dk_x dk_y \tilde{n}(k_x, k_y)} \right\}^{1/2}. \quad (7)$$

Thus the root mean square velocity of the thermal atoms is (3) given by $v_{\text{th}}^{\text{rms}} = \hbar k_{\text{th}}^{\text{rms}}/m$. On switching off the trap, that is,

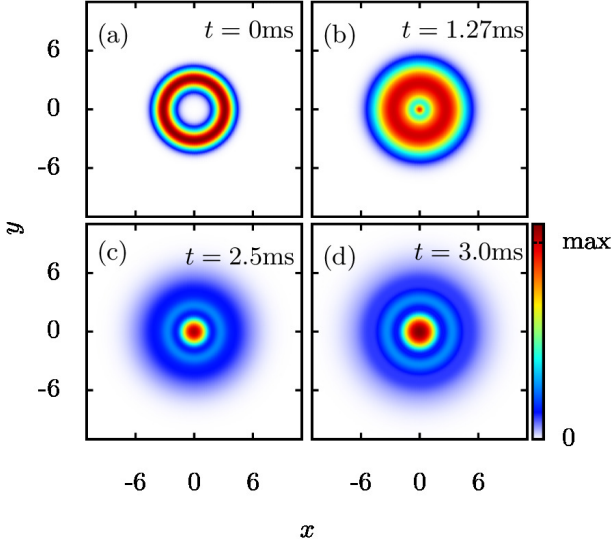


FIG. 1. (Color online) Plots showing condensate density profiles at different instants of time after release from the trap with $\Delta_x = 0$ and $T = 0$. Density is measured in units of a_{osc}^{-2} .

during free expansion of the condensate cloud in time interval δt_c , the change in the radial mean size of the thermal cloud $\delta r_{\text{th}}^{\text{rms}} = v_{\text{th}}^{\text{rms}} \times \delta t_c$. If during this time δt_c , if δr_c is the change in the radial mean size of the condensate, then the frozen thermal cloud approximation is valid when $\delta r_{\text{th}}^{\text{rms}} \ll \delta r_c$.

C. Free expansion of BEC

To simulate the time-of-flight density evolutions, we obtain the finite temperature equilibrium solutions of a single species BEC by solving Eqns. 2 and 4 self-consistently. Using the resulting condensate density implies that it has less number of atoms than the condensate density at $T = 0$, we then evolve Eq. 6 in real time using the split-step Crank-Nicolson algorithm on a 2D spatial grid. As mentioned earlier, the dynamics of \tilde{n} is neglected under this approximation, and we are interested at looking at the non-equilibrium behaviour of the condensate cloud in the presence of a static thermal background. The dimensions of the surface area considered is chosen large enough to eliminate effects of bounces from the boundaries during the free-expansion. Immediately, after the release the BEC expands along the radial direction as the inter-atomic interaction potential energy is converted to kinetic energy. For $U_0 \gg 0$ and $\Delta_x = 0$, the stationary cloud is azimuthally symmetric and multiply connected. However, when $\Delta_x \neq 0$, the azimuthal symmetry is broken, and the density evolutions are dramatically different.

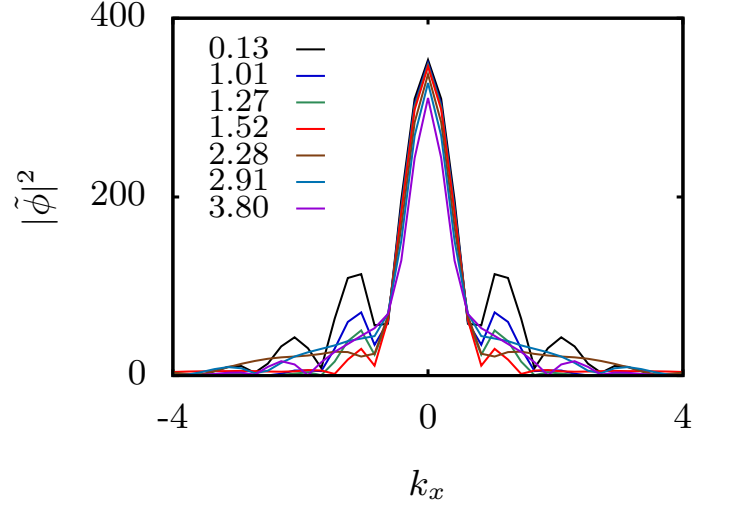


FIG. 2. (Color online) Plots showing a cut through of the momentum distribution of the atoms at different instants of time after the release of the trap with $\Delta_x = 0$ and $T = 0$.

III. RESULTS AND DISCUSSIONS

A. Zero temperature Expansion Dynamics

The typical dynamical evolution of $n_c(x, y)$ after releasing from a toroidal trapping potential is shown in Figs. 1. As to be expected at $t = 0$, $n_c(x, y)$ is toroidal in shape. After switching off the trapping potential, the release of the repulsive interaction energy creates two distinct components in the evolution. The first consists of the inner portion of the condensate which implodes towards the origin, and the second component is the the outer portion which moves outward. For the imploding component, atoms along the toroid fill up the hole initially created due to the Gaussian potential. The atoms accumulate at the center with increasing repulsive interaction energy till $n_c(0, 0)$ reaches a critical density. After attaining the critical density, the atoms expand outwards or explodes. These are the general features of the evolution after the removal of the trapping potential. However, different values of Δ_x lead to significant differences in the dynamics. In other words, separation between the minima of the oscillator potential, and the maxima of the Gaussian obstacle potential modify the expansion dynamics. In experiments $\Delta_x \neq 0$ due to gravitational sagging or due to imperfect alignment of the optical axes.

1. Coincident potential centers

For the coincident trap centers, there is a prominent self-interference between the expanding outer portion of the condensate, and the condensate cloud resulting from the repulsive explosion at the center. The interference occurs due to higher repulsive energy, and hence the velocity of expansion, accumulated at the center during the implosion. For example, in the case of $U_0 = 15\hbar\omega_x$ the central or maximum density

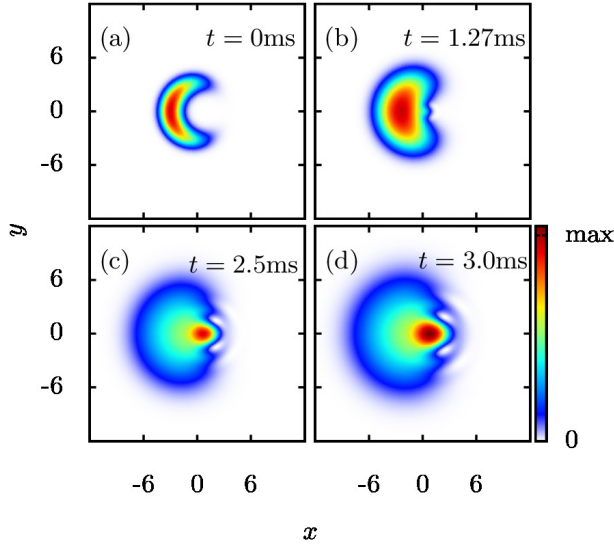


FIG. 3. (Color online) Plots showing condensate density profiles at different instants of time after release from the trap with $\Delta_x = 0.4a_{\text{osc}}$ and $T = 0$. Density is measured in units of a_{osc}^{-2} .

reaches $0.05a_{\text{osc}}$. This is more than double the maximum density, which is $\approx 0.02a_{\text{osc}}$ along the toroidal axis, in presence of the trapping potential. The self-interference results in the appearance of rings in the condensate density profile, and there is a dynamical change in the pattern as the condensate expands.

To probe the velocity distribution and release of the repulsive energy during the expansion, we compute the Fourier transform of the condensate density in the $k_x - k_y$ space. This in essence reveals the kinematic aspects of the condensate density profiles, and relates to the dynamics prior to the experimental observations based on time-of-flight (TOF) imaging. With time, the momentum distribution of the condensate atoms shrinks or broadens depending upon the release of the potential energy from the inter-atomic interaction or the mean field energy. The growth in the condensate density at the center of the trap is accompanied by a suppression of atoms with zero momentum. During the course of free expansion, the low-lying momentum peaks are suppressed, and the momentum profiles become broader. That is to say, the release of the repulsion energy leads to atoms having higher momenta. This is also evident from the plot of k_x in Fig. 2. However, as the central density reaches a critical value, which is sufficient enough to induce an expansion, the low-lying momentum peaks get washed out. Hence, there equal number of atoms for a wide range of momentum, and the interference rings start to appear in the condensate. At later times, the interference pattern becomes more prominent, and the atoms in the condensate show well defined distribution peaks in momentum. This is apparent from the presence of the peaks with higher harmonics in the Fourier spectrum.

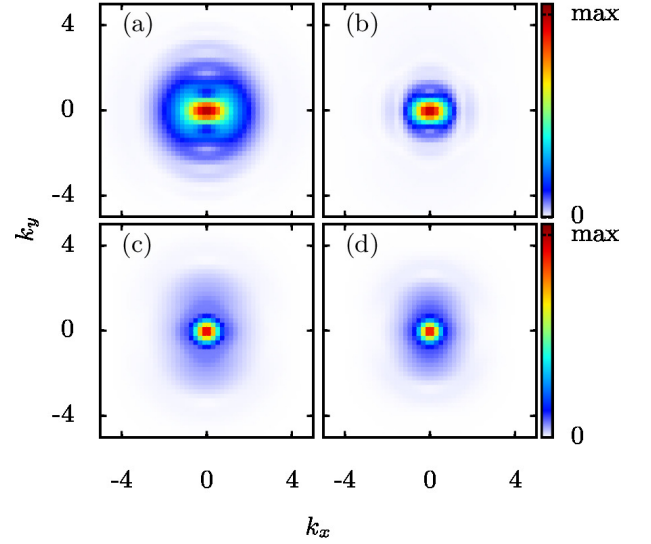


FIG. 4. Plots showing the momentum distribution of the condensate density profiles at different instants of time after release from the trap with $\Delta_x = 0.4a_{\text{osc}}$ and $T = 0$.

2. Non-coincident potential centers

When $\Delta_x \neq 0$, the rotational symmetry of the potential is broken, and the condensate cloud undergoes a transformation in topology. As Δ_x is increased, the condensate density profile assumes a bow-shaped geometry and becomes simply-connected. However, it must be mentioned here that, the simply connected profile is different from the pancake shaped condensate when $U_0 = 0$ and $\Delta_x = 0$. Hence, a difference in the dynamics of the free expansion is to be expected. At $\Delta_x = 0.4$, the equilibrium density profile of the condensate is shown in Fig. 3(a). From the figure it is evident that the density gradient along the periphery is non-uniform. As the trapping potential is removed, the condensate expands with anisotropic density and velocity distribution, and the atoms fill up the central void. As the condensate expands, the outer component continues to bear the signature of the initial density anisotropy. The inner component, on the other hand, on expansion is close to rotational symmetry.

As mentioned earlier, to probe the momentum distribution of the released atoms, we perform the Fourier transform of the condensate density in the $k_x - k_y$ space. As density distribution is anisotropic along the azimuthal direction, so is the momentum distribution. At the outset, when the density distribution assumes a banana-shaped structure with the density distribution constricted along the x -axis, and more extended along the y -axis, the momentum distribution of the atoms is more extended along the k_x . However, with the passage of time as the confining potential is switched there is a reversal of the extent of the momentum distribution. That is, at later times the momentum distribution along k_y is larger than along k_x . This is equivalent to stating that the condensate expands more along the x -direction than y -direction in the position space. This is due to the release of the repulsion energy along the x -axis which, in presence of the trapping potential, is associated

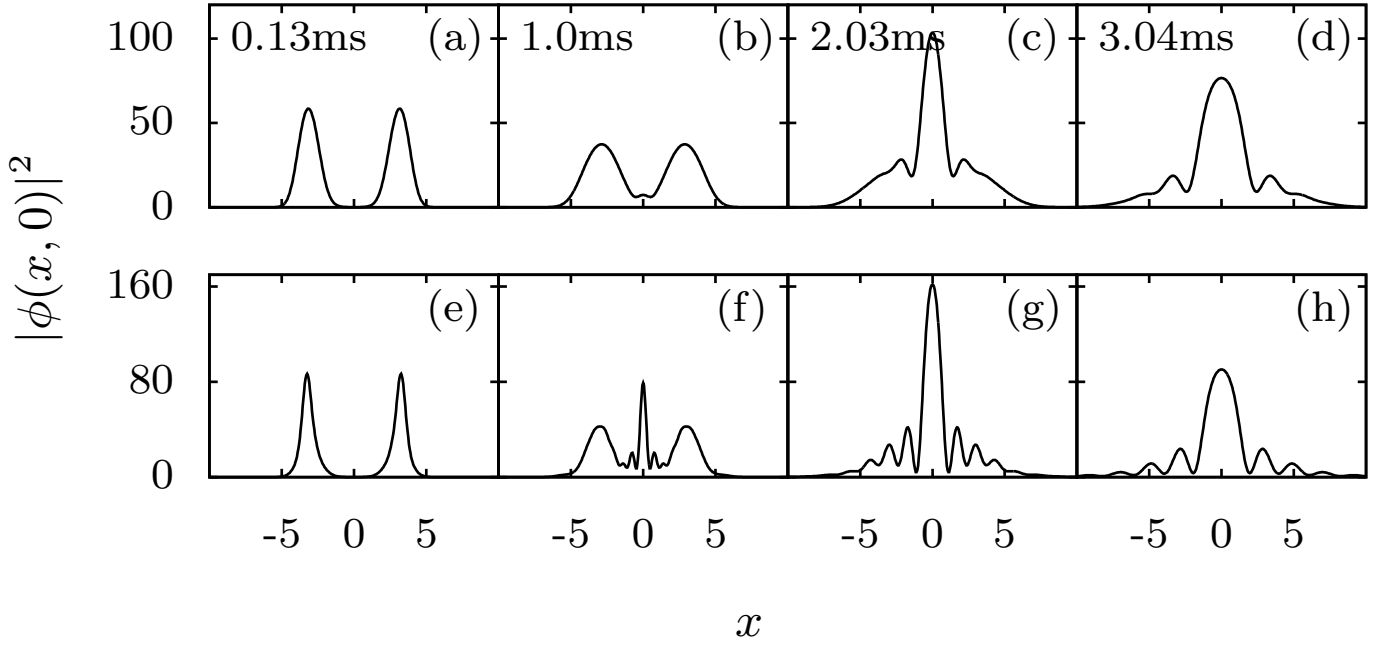


FIG. 5. (Color online) Cut through of condensate density profiles in different instants of time after release from the trap with $\Delta_x = 0$ at (a)-(d) $T = 0$, and (e)-(f) $T = 10\text{nK}$. Density is measured in units of a_{osc}^{-2} .

with higher density.

B. Finite temperature Expansion Dynamics

We study the free expansion dynamics of the toroidal condensate at $T = 10\text{nK}$ using the frozen thermal cloud approximation. For the system of our interest, the change in the radial mean size of the condensate considered during the evolution of 5 ms is $\approx 4.5a_{\text{osc}}$. The corresponding change in the thermal cloud size is $\approx 1a_{\text{osc}}$. Thus, the the condensate cloud may be assumed to move in a frozen thermal background. Based on our studies, we show that the presence of the thermal cloud brings about significant differences in the expansion dynamics of the condensate when released from the confining potential.

1. Coincident trap centers

At the outset when $t \approx 0.13\text{ms}$, that is soon after the confining potential is switched off, we find a significant difference in the structure of the condensate density profiles at $T = 0$ and $T = 10\text{nK}$. This variation in the structure of the density profiles at the early time is reflected in the subsequent stages of evolution. It is evident from Fig. 5(a) that the density profile is broader at $T = 0$ than the profile at $T = 10\text{nK}$ at $t \approx 0.13\text{ms}$. The sharp change in the density gradient associated with a narrower density profile, as seen in Fig. 5(e) at $T = 10\text{nK}$, leads to a higher kinetic energy of the atoms. As a result, on switching off the confining potential the atoms start to move inwards, and fill the void at the center with a faster rate till it reaches a density high enough so that the repulsive mean field energy

overcomes the kinetic energy. Along with this, due to the interference between the incoming and outgoing atoms at a very early stage, rings begin to appear around the center of the trap at $T = 10\text{nK}$ after $t \approx 1\text{ms}$ of evolution. This is unique to finite temperature free expansion of toroidal condensate. With further evolution in time, such that the frozen thermal cloud approximation holds good, the density at the center continues to grow with the emergence of prominent ring structures. This is not the case for $T = 0$ where there are very few ring structures. During the final stages of the evolution, as the density reaches a critical value, due to the high repulsive energy between the atoms, it explodes and starts moving away from the center.

2. Non coincident trap centers

At finite temperatures, for the non-coincident trap centers, the expansion dynamics of the condensate after switching off the confining potential is very different from the zero temperature case. As the rotational symmetry of the trap is broken, the condensate density is anisotropic in the azimuthal direction. This makes the nature of the interaction between condensate, and thermal atoms different from the case with coincident trap centers. At zero temperature, we find that the velocity of the atoms around the center of the trap is higher than the atoms located along $(x = 0, y = \pm\delta y)$. On switching off the confining potential, the maxima of the condensate density expands much faster along the +ve x direction, which at later times interfere with the atoms coming from $y = \pm\delta y$. However, at $T \neq 0$ during the free expansion, the additional repulsive interaction energy contribution from thermal atoms introduce

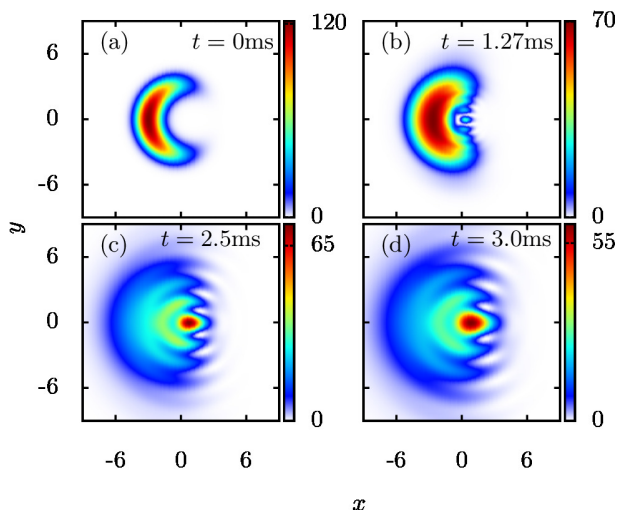


FIG. 6. (Color online) Plots showing condensate density profiles at $T = 10\text{nK}$ in different instants of time after release from the trap with $\Delta_x = 0.4a_{\text{osc}}$. Density is measured in units of a_{osc}^{-2} .

different expansion features to the condensate density profiles. The velocity of the atoms along $y \in [y - \delta y, y + \delta y]$ are similar, and they form prominent ring like structures during the expansion. This is unique to finite temperature expansion dynamics and is evident from Figs. 3, 6.

IV. CONCLUSIONS

The present studies reveal distinct features of interference patterns in the expansion dynamics of the condensates in toroidal trap configuration at zero and finite temperatures. The offset between the centers of the harmonic and Gaussian confining potentials induces topological transformation to the condensate distribution. That is, it gets transformed from a multiply (toroidal) connected to a simply connected geometry. At $T = 0$, the simply connected condensate has an expansion that is geometrically very different from the multiply connected one. Unlike in the multiply connected case, during expansion, the simply connected condensate is devoid of interference rings. The central region, which initially collapse and later expands, has an ellipsoidal density distribution. However, the outer expanding part is semi-circular in structure, and with the center shifted from the center of both the harmonic and Gaussian trapping potentials. At $T \neq 0$, because of the interaction between the condensate and thermal atoms, ring like self-interference structures are more prominent for both multiply, and simply connected condensates. The rings appear at the early stages of evolution.

ACKNOWLEDGMENTS

We thank Mark Edwards, S. Pal, K. Suthar, S. Bandyopadhyay and R. Bai for useful discussions. The results presented in the paper are based on the computations using Vikram-100, the 100TFLOP HPC Cluster at Physical Research Laboratory, Ahmedabad, India.

-
- [1] D. A. Smith, M. Gring, T. Langen, M. Kuhnert, B. Rauer, R. Geiger, T. Kitagawa, I. Mazets, E. Demler, and J. Schmiedmayer, *New J. Phys.* **15**, 075011 (2013).
 - [2] J.-y. Choi, S. W. Seo, and Y.-i. Shin, *Phys. Rev. Lett.* **110**, 175302 (2013).
 - [3] K. M. O'Hara, S. L. Hemmer, M. E. Gehm, S. R. Granade, and J. E. Thomas, *Science* **298**, 2179 (2002).
 - [4] C. A. Regal, C. Ticknor, J. L. Bohn, and D. S. Jin, *Phys. Rev. Lett.* **90**, 053201 (2003).
 - [5] C. Ryu, M. F. Andersen, P. Cladé, V. Natarajan, K. Helmerson, and W. D. Phillips, *Phys. Rev. Lett.* **99**, 260401 (2007).
 - [6] A. Ramanathan, K. C. Wright, S. R. Muniz, M. Zelan, W. T. Hill, C. J. Lobb, K. Helmerson, W. D. Phillips, and G. K. Campbell, *Phys. Rev. Lett.* **106**, 130401 (2011).
 - [7] S. Moulder, S. Beattie, R. P. Smith, N. Tammuz, and Z. Hadzibabic, *Phys. Rev. A* **86**, 013629 (2012).
 - [8] J. E. Curtis and D. G. Grier, *Phys. Rev. Lett.* **90**, 133901 (2003).
 - [9] S. Beattie, S. Moulder, R. J. Fletcher, and Z. Hadzibabic, *Phys. Rev. Lett.* **110**, 025301 (2013).
 - [10] W. H. Heathcote, E. Nugent, B. T. Sheard, and C. J. Foot, *New J. Phys.* **10**, 043012 (2008).
 - [11] O. Morizot, Y. Colombe, V. Lorent, H. Perrin, and B. M. Garraway, *Phys. Rev. A* **74**, 023617 (2006).
 - [12] J. A. Sauer, M. D. Barrett, and M. S. Chapman, *Phys. Rev. Lett.* **87**, 270401 (2001).
 - [13] S. Gupta, K. W. Murch, K. L. Moore, T. P. Purdy, and D. M. Stamper-Kurn, *Phys. Rev. Lett.* **95**, 143201 (2005).
 - [14] A. S. Arnold, C. S. Garvie, and E. Riis, *Phys. Rev. A* **73**, 041606 (2006).
 - [15] B. E. Sherlock, M. Gildemeister, E. Owen, E. Nugent, and C. J. Foot, *Phys. Rev. A* **83**, 043408 (2011).
 - [16] K. Henderson, C. Ryu, C. MacCormick, and M. G. Boshier, *New J. Phys.* **11**, 043030 (2009).
 - [17] T. A. Bell, J. A. P. Glidden, L. Humbert, M. W. J. Bromley, S. A. Haine, M. J. Davis, T. W. Neely, M. A. Baker, and H. Rubinsztein-Dunlop, *New J. Phys.* **18**, 035003 (2016).
 - [18] G. E. Marti, R. Olf, and D. M. Stamper-Kurn, *Phys. Rev. A* **91**, 013602 (2015).
 - [19] A. Kumar, N. Anderson, W. D. Phillips, S. Eckel, G. K. Campbell, and S. Stringari, *New J. Phys.* **18**, 025001 (2016).
 - [20] C. Ryu, P. W. Blackburn, A. A. Blinova, and M. G. Boshier, *Phys. Rev. Lett.* **111**, 205301 (2013).
 - [21] R. Mathew, A. Kumar, S. Eckel, F. Jendrzejewski, G. K. Campbell, M. Edwards, and E. Tiesinga, *Phys. Rev. A* **92**, 033602 (2015).
 - [22] K. C. Wright, R. B. Blakestad, C. J. Lobb, W. D. Phillips, and G. K. Campbell, *Phys. Rev. A* **88**, 063633 (2013).
 - [23] N. Murray, M. Krygier, M. Edwards, K. C. Wright, G. K. Campbell, and C. W. Clark, *Phys. Rev. A* **88**, 053615 (2013).
 - [24] A. Roy and D. Angom, *New J. Phys.* **18**, 083007 (2016).

- [25] M. Zawada, R. Abdoul, J. Chwedeczek, R. Gartman, J. Szczepkowski, . Tracewski, M. Witkowski, and W. Gawlik, *J. Phys. B* **41**, 241001 (2008).
- [26] K. Gawryluk, M. Brewczyk, M. Gajda, and K. Rzewski, *J. Phys. B* **43**, 105303 (2010).
- [27] A. Roy and D. Angom, *Phys. Rev. A* **92**, 011601(R) (2015).
- [28] A. Roy, S. Gautam, and D. Angom, *Phys. Rev. A* **89**, 013617 (2014).
- [29] A. Roy and D. Angom, *Phys. Rev. A* **90**, 023612 (2014).